Hindawi
Geofluids
Volume 2023, Article ID 2557871, 9 pages
https://doi.org/10.1155/2023/2557871

Research Article

Analysis of the Influence of Hydraulic Fracturing Fluid Velocity on Fracture Propagation

Yuan Wang,[1,2,3] **Liguo Zhong**,[1] **Xiaoguang Sun**,[3] **Yanqing Feng**,[2,3] **and Haikun Lin**[2,3]

[1]*Unconventional Oil and Gas Institute, China University of Petroleum, Beijing 102249, China*
[2]*China United Coalbed Methane National Engineering Research Center Co., Ltd., Beijing 100095, China*
[3]*PetroChina Coalbed Methane Company Limited, Beijing 100028, China*

Correspondence should be addressed to Yuan Wang; wangyuan_cbm@petrochina.com.cn

Received 27 October 2022; Revised 27 November 2022; Accepted 18 March 2023; Published 19 May 2023

Academic Editor: Peng Tan

To reveal the influence of fracturing fluid velocity on hydraulic fracturing fracture propagation, a hydraulic fracturing numerical model was established based on a coalbed methane (CBM) field in the northeast of China. The influence of fracturing fluid velocity on hydraulic fracturing fracture propagation is mainly investigated, and the relationship between fracturing fluid velocity and fracture tip displacement is obtained. The results show that the fracture front presents different morphological characteristics at different times of fracturing. The larger the fracturing fluid velocity, the larger the fracture length and width after the same time of hydraulic fracturing. However, the fracture length will not increase indefinitely; the fracture will stop spreading when the injected fluid reaches a balance with the fluid that is permeated or filtered from the fracture surface. With the increase in fracturing fluid velocity, the fracture length increases logarithmically and gradually flattens out. The research conclusion provides a certain reference for improving the fracture propagation effect of hydraulic fracturing.

1. Introduction

The resources of coalbed methane (CBM) in China are about $35 \times 10^{12}\ m^3$, and the CBM content of a low-rank coal reservoir is about $16 \times 10^{12}\ m^3$, accounting for more than 47% [1]. Currently, the production of CBM wells is generally low in China, which is largely related to the poor conditions of the coalbed methane reservoir. CBM reservoirs in China are generallycharacterized by low reservoir pressure, low initial permeability, low gas saturation and poor homogeneity, due to the influence of several tectonic movements. Especially for the shallow coalbed methane reservoir, it is verydifficult for desorption and migration of CBM due to the low reservoir pressure.[2]. In low permeability coal seam, the effect of using natural gas seepage migration law to preextract gas is poor, so it is usually necessary to take some artificial methods to increase the permeability of coal rock. The commonly used methods mainly include the loosening blasting method and the hydraulic fracturing method [3]. Hydraulic fracturing is the most widely used method.

Hydraulic fracturing is the use of high water pressure inside the borehole to destroy the surrounding rock of the borehole wall, resulting in the initiation and expansion of cracks around the borehole, forming a certain scale of a fracture network and forming a pressure-relief zone around the fracture, thus increasing the permeability of coal rock. After fracturing, many widely distributed hydraulic fractures can appear in the coal seam, which causes a large area of pressure drop around the well hole when the gas is extracted from the well. The surface area of gas desorption caused by the pressure drop of the coal seam is increased, which ensures the rapid and relatively lasting discharge of coalbed methane. The gas production is about 5-20 times higher than that before fracturing, and the recovery effect is very significant [4].

In terms of the fracture propagation mechanism of hydraulic fracturing, many researchers have carried out a lot of research in numerical simulation and physical tests. Warpinski used the stress ring device to monitor the fracture propagation process during the mine test in real time and found that the main fracture and branch fracture were

extended simultaneously during fracturing [5]. Behrmann and Nolte conducted triaxial hydraulic fracturing test research and found that hydraulic fractures would initiate and expand along the direction of the minimum principal stress [6]. Shicheng et al. used CT to observe and analyze the internal fractures of the fractured samples and found that the fracturing fluid displacement and fracturing fluid viscosity are conducive to the formation of complex fractures within a certain range, and either too high or too low will have negative effects. When the ground stress difference is low, hydraulic fractures easily crack directly along the natural fractures [7]. The effect of the high stress difference is favorable for more natural fractures to form a relatively complex fracture net structure. Hou et al. studied the communication behavior between hydraulic fractures and natural fractures during fracturing and found that whether hydraulic fractures can penetrate natural fractures is mainly related to the opening and cementation degree of natural fractures [8]. Natural fractures with a large opening and low cementation strength are easy to turn along hydraulic fractures and not easy to form complex fractures. The interaction between hydraulic fractures and natural fractures forms a spatial nonplanar fracture network.

However, the actual cleaved fractures in coal seams are very developed, and natural fractures, bedding planes, and structural planes have a great influence on the expansion morphology of hydraulic fractures, leading to the formation of three-dimensional hydraulic fractures in the actual reservoir that will be very complex, and many fracture branches may occur. The vertical extension of hydraulic fractures in coal reservoirs is easily limited by the thickness of coal seams [9].

Some scholars have found that when the bottomhole pressure exceeds the vertical ground stress, horizontal fracture components are prone to occur at the interface between the coal seam and the adjacent roof and floor strata, resulting in T- or H-type fractures [10, 11]. Thiercelin et al. found that the smaller the fracture toughness of rock strata, the easier it is for hydraulic fractures to spread in it [12]. On the contrary, the greater the fracture toughness of the rock layer, the greater the pressure required for fracture propagation. According to the theory of linear elastic fracture mechanics, Simonson et al. proved that the hydraulic fractures in the rock strata with higher Young's modulus could extend to the critical rock strata with lower Young's modulus. In contrast, the propagation of hydraulic fractures in rocks with lower Young's modulus is limited by critical rocks with higher Young's modulus [13]. Chen et al. studied the complex fracture of a T-shaped fracture generated by a coal seam by establishing a mathematical model, controlling flow, and single-factor analysis and obtained the extension rule of a T-shaped fracture in the coal seam [14]. Deng et al. used the Griffith theory and hydraulic fracturing method to analyze the hydraulic fracture propagation process of rock mass pore wall in the stress field, the relationship between the original stress field, the propagation pressure of cracks containing internal pressure, and the mechanical properties of surrounding rock [15].

The previous researches mainly focus on the hydraulic fracture geometry and extension law of the hydraulic fracturing test. However, the fracturing fluid velocity is one of the important parameters affecting hydraulic fracturing. Under different fracturing fluid velocities, the fracture initiation modes are also different; that is, the fracturing fluid velocity and other factors will affect the evolution characteristics of the hydraulic fracturing fracture initiation. However, the current research on the relationship between the fracturing fluid velocity and the initiation and propagation of hydraulic fractures is insufficient.

Therefore, this paper takes a coalbed methane field in China as the research background, through the numerical simulation method to study the fracture propagation of different pump injection rates in the process of hydraulic fracturing and explore its regularity with hydraulic fracturing, which has certain guiding significance for improving the effect of hydraulic fracturing.

2. Engineering Overview

CBM field is located in Yanbian Korean Autonomous Prefecture in the east of Jilin Province, adjacent to the Tumen River in the west, Hulu Turtle in the east, Songshu Village in the north, and the China-Russia border in the south, covering an area of about 630 km^2. Hunchun River is located from the northeast across the basin, flowing southwest, into the Tumen River. The plain is 21-80 m above sea level, and the hilly area is 80-260 m above sea level. Most of them are cut into gullies and ridges by south-north streams. In the west of the basin, there are Baliancheng, Chengxi, Sandaoling, and Yingan mining areas. In the south is the detailed exploration district of Baishi #1, #2, and #3. In the east, there are Tuohezi, Wujiazi census areas, and Miaoling mining area (Figure 1). Among them, the predicted coalbed methane resources of the gas field can reach19.6×10^8 m^3, which is a block with good prospects for the exploration and development of low-rank coal CBM in China.

The widely developed coal seams in the whole area include 19, 20, 21, 22, 23, 26, and 30 coal seams. The thickness of single-layer coal is generally 0.2-3.0 m, and the maximum thickness is 8.5 m. The cumulative thickness is generally 5-40 m, with a maximum thickness of 43.44 m, which is characterized by a thin coal seam and many layers (Figure 2). The burial depth of coal seam is larger in the west than in the east. From west to east, coal is long flame coal, long flame coal-lignite, lignite, and bottom-up coal is long flame coal, lignite. The coal accumulation center is located in the east of Balancheng, the middle of the west of the city, and the north of the Banshi district #1 area. The cumulative thickness of the coal seam is more than 20 m, the coal layers are many, and the distribution is stable. The coal seam becomes thinner and less continuous in the east. The burial depth of the coal seam in the west is larger than that in the east, but the burial depth of the main coal seam is generally less than 600 m, which is very suitable for the development of CBM.

3. Mechanical Model of Hydraulic Fracturing of CBM Field

3.1. Cohesion-Displacement Equation of Bonding Element. It is assumed that fracture propagation is controlled by the

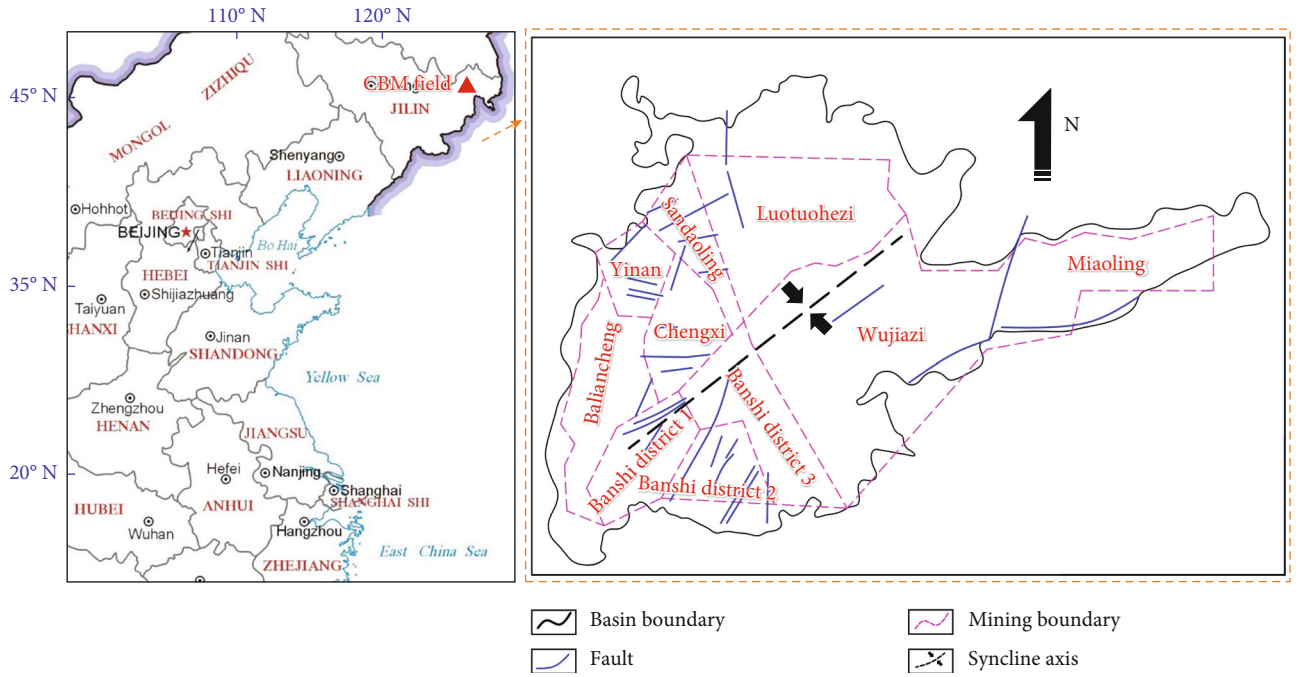

Figure 1: Tectonic outline of Hunchun basin.

Legend	Thickness (m)	Lithology
	0–20	Sandy soil
	20–400	Conglomerate, sandstone, siltstone, mudstone, coal
	450–800	Conglomerate, carbonaceous mudstone contains 70 layers of coal
	100–200	Conglomerate, sandstone, coal
	1300	Andesite, conglomerate

Figure 2: Comprehensive column of Hunchun basin.

bond zone model [16, 17]. The model requires a predefined fracture propagation path composed of bond elements, and later fractures will expand along the predefined expansion path. The model is based on Zheltov and Khristianovitch's assumption that the load acting on the fracture should ensure the boundedness of crack tip stress [18]. The bond zone model consists of two parts: one is the cohesion-displacement equation which controls the fracture propagation and the other is the hydrodynamic equation which describes the fluid flow in the fracture and osmotic filtration to the rock interior [19].

The bond zone is located at the tip of the fracture, and the cohesion force should resist the tension inside the fracture and counteract the stress singularity at the tip. The region near the fracture tip undergoes plastic deformation and microfracture process under the action of hydraulic tension, which is a transition region between the fracture and undamaged rock. In the bond zone model, the shape of a fracture tip is not completely sharp, which can avoid the singular phenomenon of fracture tip stress.

The zero-thickness cohesive element has been used in this paper, i.e., the geometric thickness of the element is set to zero, by which more accurate model results could be obtained. Figure 3 shows the bond element and its relationship with the adjacent finite element [20]. Bonding elements share or bind binding constraints with nodes of surface elements in adjacent areas. Different from the conventional bonding element, there are pore pressure nodes between the upper and lower adjacent nodes of the bonding element, which are used to describe the mechanical characteristics of the fluid pressure acting on the bonding element surface. The pore pressure node has no displacement degrees of freedom but only pore pressure degrees of freedom.

The cohesion-displacement model assumes that the rock is linear elastic before damage occurs, and the damage occurs and evolves after a certain displacement/stress

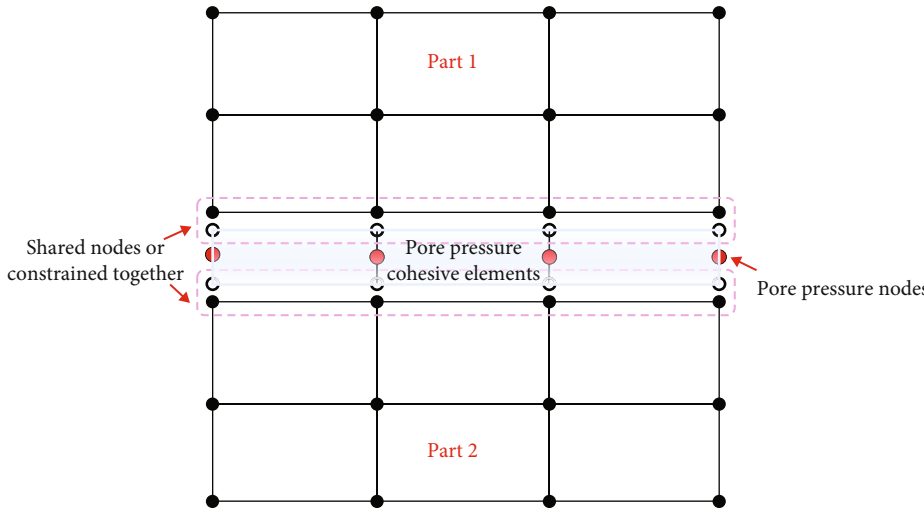

Figure 3: The pore pressure cohesive elements.

condition is reached. The elastic constitutive relation of rock is shown in the following equation:

$$\begin{Bmatrix} t_n \\ t_s \\ t_t \end{Bmatrix} = \frac{E(1-\nu)}{(1+\nu)(1-2\nu)} \begin{bmatrix} 1 & 0 & 0 \\ 0 & \dfrac{1-2\nu}{2(1-\nu)} & 0 \\ 0 & 0 & \dfrac{1-2\nu}{2(1-\nu)} \end{bmatrix} \begin{Bmatrix} \varepsilon_n \\ \varepsilon_s \\ \varepsilon_t \end{Bmatrix}, \tag{1}$$

where t_n is the tension perpendicular to the fracture surface and t_s and t_t are the shear forces in two directions parallel to the fracture surface.

Figure 4 shows the cohesion-displacement criterion of the bonding element [20]. At the initial stage of hydraulic fracturing, the cohesion of the crack tip increases linearly with the increase in the displacement of the upper and lower fracture surfaces. When the surface displacement of the upper and lower fractures reaches δ^0, the cohesion reaches the critical stress, which is the bond strength of the bonding element t^0. When the displacement is greater than δ^0, the cohesion force at the fracture tip follows an irreversible linear damage evolution law due to material damage. When the displacement is δ^f, the cohesion is 0, and the fracture is completely split. The region below the cohesion-displacement curve represents the fracture energy, G_c.

When damage occurs inside the rock, the strength also begins to degrade. When the stress/strain inside the rock reaches the specified initial damage criterion, the strength of the rock decreases gradually. The initial damage criterion of rock in this paper is the quadratic normal stress criterion [21], as shown in

$$\left\{\frac{\langle t_n\rangle}{t_n^0}\right\}^2 + \left\{\frac{t_s}{t_s^0}\right\}^2 + \left\{\frac{t_t}{t_t^0}\right\}^2 = 1, \langle t_n\rangle = \frac{(t_n + |t_n|)}{2}, \tag{2}$$

where t_n^0, t_s^0, and t_t^0 represent the peak strength of the normal stress of rock that should be reached when the crack expands only along the vertical fracture plane or only along the two shear directions parallel to the fracture plane, respectively. The Macaulay bracket operator "<>" is used to specify that the rock will not be damaged under compressive stress or deformation.

The damage evolution law describes the degradation rate of material strength when the specified initial damage criterion is satisfied. The stress component in the cohesion-displacement model after rock damage is as follows:

$$\begin{aligned} t_n &= \begin{cases} (1-D)\overline{t_n}, & \overline{t_n} \geq 0 \\ \overline{t_n}, & \overline{t_n} < 0 (\text{It is assumed that no damage occurs when the rock is pressed.}) \end{cases}, \\ t_s &= (1-D)\overline{t_s}, \\ t_t &= (1-D)\overline{t_t}, \end{aligned} \tag{3}$$

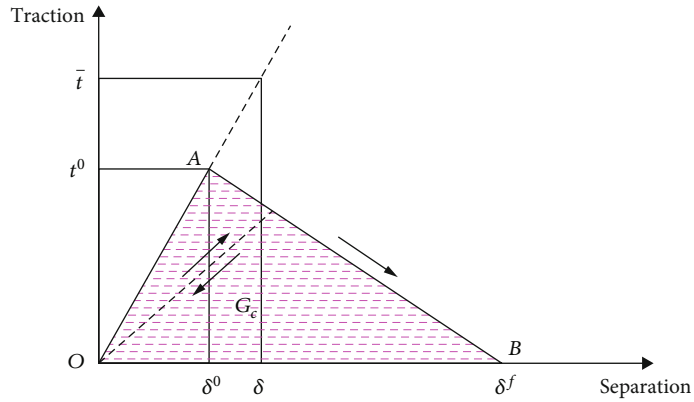

Figure 4: The traction-separation criterion.

where $\overline{t_n}$, $\overline{t_s}$, and $\overline{t_t}$, respectively, represent the stress components determined according to the cohesion-displacement criterion assuming no damage to the rock material, as shown in Figure 4. D is the damage factor, which represents the damage degree of rock material. After rock damage occurs, the damage factor changes monotonically from 0 to 1 with the increase in load. In this paper, the rock material accords with the law of linear damage evolution.

$$D = \frac{\delta_m^f\left(\delta_m^{\max} - \delta_m^0\right)}{\delta_m^{\max}\left(\delta_m^f - \delta_m^0\right)}, \tag{4}$$

where δ_m represents the effective displacement, and the mathematical expression is as follows:

$$\delta_m = \sqrt{\langle\delta_n\rangle^2 + {\delta_s}^2 + {\delta_t}^2}. \tag{5}$$

In Equation (4), δ_m^f represents the effective displacement when the rock is completely damaged; δ_m^0 represents the effective displacement of the initial rock damage; $\delta_m^{\max}$ represents the maximum effective displacement experienced by the rock during its loading history.

3.2. Equation of Fluid Dynamics. The fluid in the fracture is assumed to be incompressible. The fluid flows in the hydraulic fracture along two directions: one is tangential flow, that is, the direction parallel to the fracture surface, which is used to simulate the fluid flow in the hydraulic fracture in the expansion direction. The other is vertical flow, that is, the direction perpendicular to the fracture surface, which is used to model fluid exchange between the permeable fracture surface and the porous media rock mass.

The fluid parallel to the fracture surface is assumed to be a Newtonian fluid, and the flow rate is controlled by the lubrication equation derived from the Navier-Stokes equation in the following form [22]:

$$\mathrm{qd} = -k_t \nabla p. \tag{6}$$

According to the Reynolds equation, tangential permeability can be defined as follows:

$$k_t = \frac{d^3}{12\mu}. \tag{7}$$

According to the conservation equation of fluid mass, the following can be obtained:

$$\frac{\partial d}{\partial t} + \nabla \cdot (\mathrm{qd}) + (q_t + q_b) = Q_{\mathrm{inj}}, \tag{8}$$

where q is the fluid velocity, k_t is tangential permeability, ∇p is the fluid pressure gradient along the fracture direction, d is crack opening, μ is fluid viscosity, Q_{inj} is the pumping flow rate, and q_t and q_b are the vertical flow velocities flowing into the upper and lower fracture surfaces, respectively, reflecting the fluid filtration loss from the fracture to the rock.

The vertical flow is expressed as follows:

$$\begin{aligned} q_t &= c_t(p - p_t), \\ q_b &= c_b(p - p_b), \end{aligned} \tag{9}$$

where c_t and c_b are, respectively, the fluid loss coefficients of the upper and lower surfaces of the bonding unit. p_t and p_b are pore pressures in rock units, respectively. p is the fluid pressure acting on the fracture surface.

4. Numerical Simulation

4.1. Modeling. The regularity of fracture initiation and propagation in the process of reservoir hydraulic fracturing has always been the focus of many scholars. The effect of hydraulic fracturing directly determines the productivity of coalbed methane and the recovery rate of CBM. Taking a coalbed methane field in China as the background, the variation characteristics of fracturing fluid velocity during the process of hydraulic fracture propagation are studied by numerical simulation (See Figure 5) [23–25]. The permeability of coal samples under different pore pressures was tested by the steady-state permeability testing method. The porosity

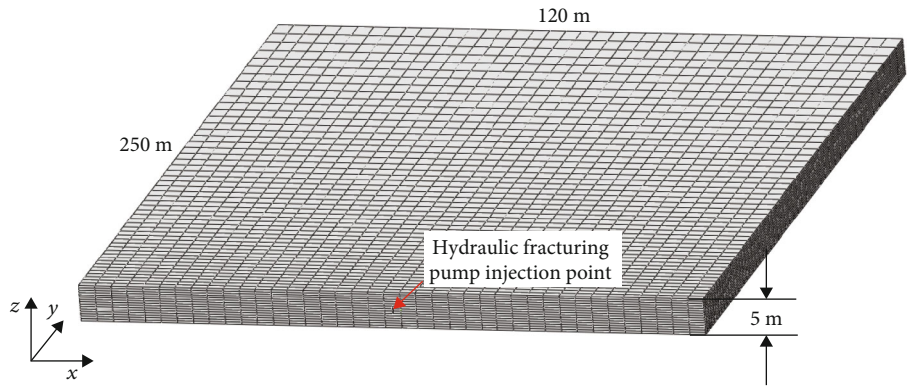

Figure 5: Model diagram of hydraulic fracture.

Table 1: Main model parameters.

Permeability (mD)	Tensile strength t (MPa)	Young's modulus E (GPa)	Porosity	Poisson's ratio μ	Filtration coefficient ($\times 10^{-13}$ m/Pa.s)	Fluid viscosity (Pa.s)
0.034	1.6	4.71	0.110	0.26	4.30	0.10

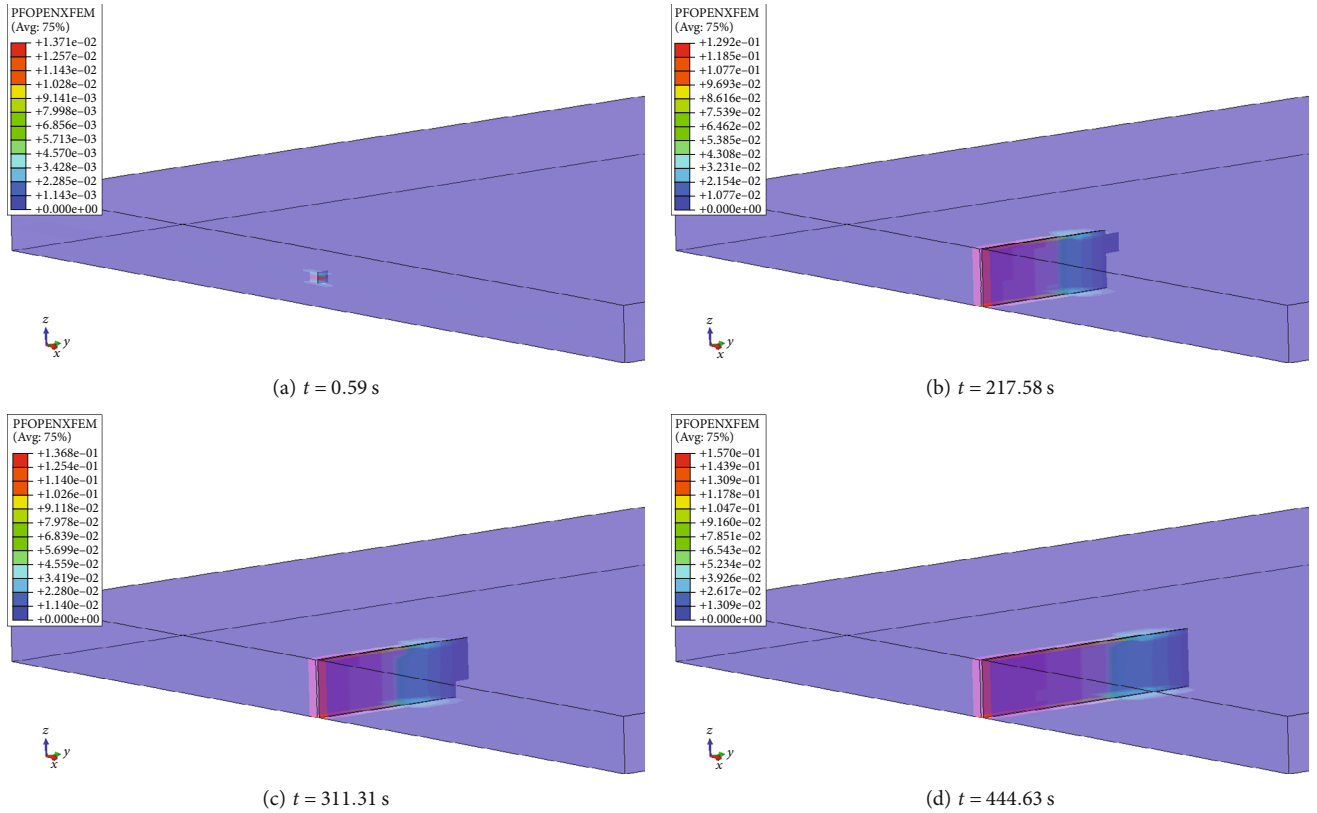

Figure 6: The results of hydraulic fractures in coal seams at different times when fluid velocity is 0.117 m^3/s.

of the coal was obtained by a mercury injection test. The main parameters of the model are shown in Table 1. The minimum horizontal stress σ_x is 7.2 MPa, the maximum horizontal stress σ_y is 9.0 MPa, and the vertical stress σ_z is 8.1 MPa.

4.2. Results and Analysis. Figure 6 shows the results of hydraulic fracture propagation in coal seam at different times when the fracturing fluid velocity is 0.117 m^3/s. The PFOPENXFEM parameter in the figure represents the fracture width (fracture opening) at each point on the fracture. At 0.59 s, the fracture begins to crack. Since the minimum horizontal principal stress is along the x-direction, the fracture plane is parallel to the yoz plane. At different times, the fracture front presents different morphological characteristics: as shown in Figure 6(b), the fracture front is inside the coal seam; as shown in Figure 6(c), the upper (or lower)

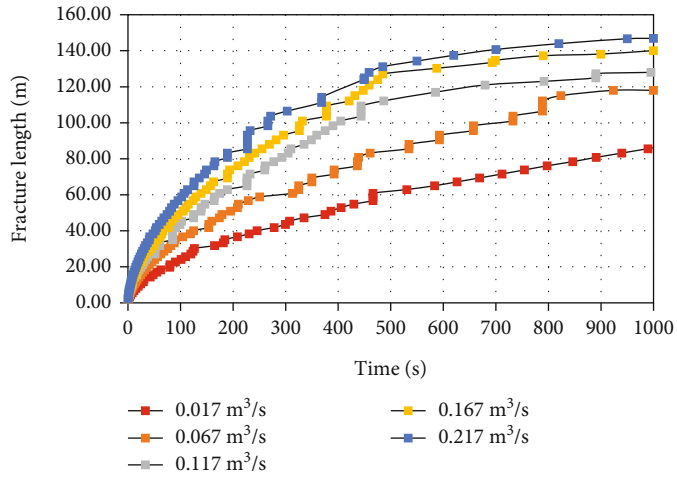

Figure 7: Fracture length at different fracturing fluid velocities.

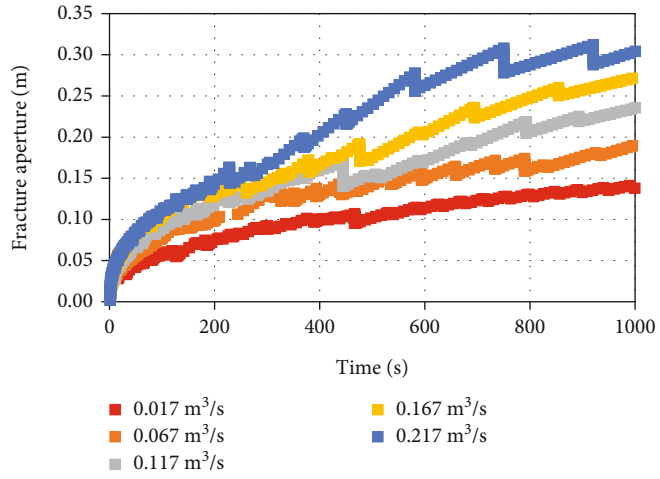

Figure 8: Fracture width at the injection point at different fracturing fluid velocities.

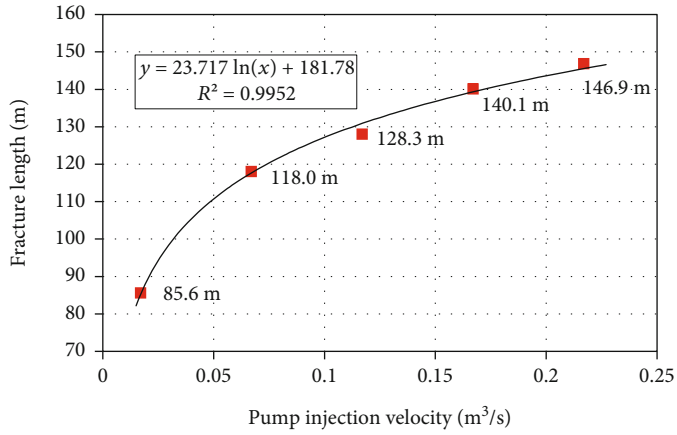

Figure 9: Fracture length at different pumping rates when fluid is injected 1000 s.

part of the coal seam is connected with the internal crack and is at the most front; as shown in Figure 6(d), the maximum seam length at the upper and lower points in the coal seam is the same. However, in any case, due to the thin coal seam (5 m) simulated in this paper, there is little difference in the fracture length corresponding to each point at the front of the fracture during the process of hydraulic fracture expansion, and there is no great difference between the

upper and lower fracture lengths and the middle fracture lengths. The seam width of each point in the direction of the seam height is basically the same.

The fracture propagation at different times at different fracturing fluid velocities was calculated. Figures 7 and 8 show the results of the fracture length and the fracture width at the pumping point at different fracturing fluid velocities, respectively. As can be seen from the figure, the larger the fracturing fluid velocity, the larger the fracture length and width after the same time of hydraulic fracturing. However, with the increase in time, the fracture length will not increase indefinitely; the fracture will stop spreading when the injected fluid reaches a balance with the fluid that is permeated or filtered from the fracture surface.

As shown in Figure 7, with the increase in pumping time, the fracture length gradually approaches a certain limit value, and the corresponding limit value is different for different fracturing fluid velocities. The greater the fracturing fluid velocity, the greater the fracture length limit, because the higher the fracturing fluid velocity, the greater the fluid loss is required to achieve dynamic equilibrium with it.

Figure 9 shows the fracture length after 1000 s of hydraulic fracturing at different fracturing fluid velocities. As can be seen from the figure, with the increase in the fracturing fluid velocity, the fracture length increased in a logarithmic pattern (Equation (10)) and finally gradually tended to be flat.

$$y = 23.71 \ln(x) + 181.78, \quad R^2 = 0.99, \tag{10}$$

where y is the fracture length (m) and x is the fracturing fluid velocity ($m.s^{-2}$).

5. Conclusions

Based on the background of the coalbed methane (CBM) field in the northeast of China, the numerical analysis method is used to investigate the fracture propagation of different fracturing fluid velocities during hydraulic fracturing. The following main conclusions were reached:

(1) The fracture front presents different morphological characteristics at different times of fracturing. The larger the fracturing fluid velocity, the larger the fracture length and width after the same time of hydraulic fracturing

(2) The fracture length will not increase indefinitely. The fracture will stop spreading when the injected fluid reaches a balance with the fluid that is permeated or filtered from the fracture surface

(3) With the increase in fracturing fluid velocity, the fracture length increases logarithmically and gradually flattens out

Data Availability

All data used during this study are available from the corresponding author by request.

Conflicts of Interest

The authors declare that they have no conflict of interest.

Acknowledgments

This study was supported by the National Science and Technology Major Project of the Ministry of Science and Technology of China (Grant No. 2016ZX05042).

References

[1] H. Z. Song, *Study on the Distribution Characteristics and the Exploration and Development Prospect of Coal Resource of China*, China University of Geosciences, Beijing, 2013.

[2] Y. P. Zhang, Z. M. Yang, and B. A. Xian, "Coal-bed gas stimulation technology," *Special Oil & Gas Reservoirs*, vol. 13, no. 1, pp. 95–98, 2006.

[3] D. Y. Guo, H. B. Pei, J. C. Song, F. Q. Qing, and X. B. Liu, "Study on spliting mechanism of coal bed deep-hole cumulative blasting to improve permeability," *Journal of China Coal Society*, vol. 33, no. 12, pp. 1381–1395, 2008.

[4] T. T. Luo, *Coal Rock Characteristics and Fracturing Metholds for QinShui Reservoir*, Chengdu University of Technology, Sichuan, 2010.

[5] N. R. Warpinski, "Hydraulic fracturing in tight, fissured media," *Journal of Petroleum Technology*, vol. 43, no. 2, pp. 146–209, 1991.

[6] L. A. Behrmann and K. G. Nolte, "Perforating requirements for fracture stimulations," *SPE Drilling & Completion*, vol. 14, no. 4, pp. 228–234, 1999.

[7] Z. H. Shicheng, G. U. Tiankui, Z. H. Tong, Z. Yushi, and M. Songru, "Fracture propagation mechanism experiment of hydraulic fracturing in natural shale," *Acta Petrolei Sinica*, vol. 35, no. 3, pp. 496–503, 2014.

[8] B. Hou, W. Cheng, M. Chen, Y. S. Zou, and S. R. Mu, "Experiments on the non-planar extension of hydraulic fractures in fractured shale gas reservoirs," *Natural Gas Industry*, vol. 34, no. 12, pp. 81–86, 2014.

[9] J. Zou, Y. Y. Jiao, F. Tan, J. Lv, and Q. Zhang, "Complex hydraulic-fracture-network propagation in a naturally fractured reservoir," *Computers and Geotechnics*, vol. 135, article 104165, 2021.

[10] S. N. Gulrajani and K. G. Nolte, "Fracture evaluation using pressure diagnostics," *Reservoir Stimulation*, vol. 9, 2000.

[11] R. G. Jeffrey and X. Zhang, "Hydraulic fracture growth in coal," in *SHIRMS 2008: Proceedings of the first southern hemisphere international rock mechanics symposium*, pp. 369–379, Australian Centre for Geomechanics, Perth, 2008.

[12] M. Thiercelin, R. G. Jeffrey, and K. B. Naceur, "Influence of fracture toughness on the geometry of hydraulic fractures," *SPE Production Engineering*, vol. 4, no. 4, pp. 435–442, 1989.

[13] E. R. Simonson, A. S. Abou-Sayed, and R. J. Clifton, "Containment of massive hydraulic fractures," *Society of Petroleum Engineers Journal*, vol. 18, no. 1, pp. 27–32, 1978.

[14] Y. F. Cheng, B. L. Wu, N. Li, Y. Zheng, and X. Wang, "Analysis of hydraulic fracture extension and influencing factors in coal seam," *Special Oil & Gas Reservoirs*, vol. 20, no. 2, pp. 126–130, 2013.

[15] G. Z. Deng, B. X. Huang, G. D. Wang, and H. J. Liao, "Theoretical analysis of crack expanding under pore hydraulic pressure," *Journal of Xi'an University of Science and Technology*, vol. 23, no. 4, pp. 261–264, 2003.

[16] D. S. Dugdale, "Yielding of steel sheets containing slits," *Journal of the Mechanics and Physics of Solids*, vol. 8, no. 2, pp. 100–104, 1960.

[17] G. I. Barenblatt, "The mathematical theory of equilibrium cracks in brittle fracture," *Advances in Applied Mechanics*, vol. 7, pp. 55–129, 1962.

[18] Y. Zheltov and S. Khristianovitch, *On the Mechanism of Hydraulic Fracturing of an Oil-Bearing Stratum*, vol. 5, Izvest Akad Nauk SSR, OTN, 1955.

[19] Z. Chen, R. G. Jeffrey, and X. Zhang, "Numerical modeling of three-dimensional T-shaped hydraulic fractures in coal seams using a cohesive zone finite element model," *Hydraulic Fracturing Journal*, vol. 2, no. 2, pp. 20–37, 2015.

[20] J. P. Zou, W. Z. Chen, J. Q. Yuan, D. S. Yang, and J. P. Yang, "3-D numerical simulation of hydraulic fracturing in a CBM reservoir," *Journal of Natural Gas Science and Engineering*, vol. 37, pp. 386–396, 2017.

[21] P. P. Camanho and C. G. Dávila, *Mixed-Mode Decohesion Finite Elements for the Simulation of Delamination in Composite Materials*, Tech Rep NASA/TM-2002-211737, 2002.

[22] R. W. Zimmerman, S. Kumar, and G. S. Bodvarsson, "Lubrication theory analysis of the permeability of rough-walled fractures," *International Journal of Rock Mechanics and Mining Sciences*, vol. 28, no. 4, pp. 325–331, 1991.

[23] J. P. Tang and T. Qi, "Analysis of fracturing fluid flow velocity influence on shale volume fracturing crack propagation," *Journal of Liaoning Technical University (Natural Science)*, vol. 38, no. 1, pp. 44–51, 2019.

[24] J. Zou, X. Hu, Y. Y. Jiao et al., "Dynamic mechanical behaviors of rock's joints quantified by repeated impact loading experiments with digital imagery," *Rock Mechanics and Rock Engineering*, vol. 55, no. 11, pp. 7035–7048, 2022.

[25] J. Zou, K. Wu, X. Zhang et al., "Effective evaluation of deep-hole blasting for controlling strong tremors induced by deep coal mining-a case study," *International Journal of Rock Mechanics and Mining Sciences*, vol. 159, article 105211, 2022.